AGU PUBLICATIONS

Water Resources Research

RESEARCH ARTICLE
10.1002/2014WR015687

Key Points:
- Empirical models are developed to simulate 18O of monthly precipitation
- Precipitable water content describes the most variance in precipitation 18O
- Uncertainty in modeling monthly and long-term precipitation 18O is assessed

Supporting Information:
- Supporting Information S1
- Table S1
- Table S2

Correspondence to:
C. Delavau,
umdelav0@cc.umanitoba.ca

Citation:
Delavau, C., K. P. Chun, T. Stadnyk, S. J. Birks, and J. M. Welker (2015), North American precipitation isotope (δ^{18}O) zones revealed in time series modeling across Canada and northern United States, *Water Resour. Res.*, *51*, 1284–1299, doi:10.1002/2014WR015687.

Received 8 APR 2014
Accepted 22 JAN 2015
Accepted article online 28 JAN 2015
Published online 27 FEB 2015

North American precipitation isotope (δ^{18}O) zones revealed in time series modeling across Canada and northern United States

C. Delavau[1], K. P. Chun[2], T. Stadnyk[1], S. J. Birks[3], and J. M. Welker[4]

[1]Department of Civil Engineering (Water Resources), University of Manitoba, EITC E1-368A Engineering, Winnipeg, Manitoba, Canada, [2]Global Institute for Water Security, University of Saskatchewan, Saskatoon, Saskatchewan, Canada, [3]Alberta Innovates-Technology Futures, Calgary, Alberta, Canada, [4]Biological Sciences, University of Alaska Anchorage, Anchorage, Alaska, USA

Abstract Delineating spatial patterns of precipitation isotopes ("isoscapes") is becoming increasingly important to understand the processes governing the modern water isotope cycle and their application to migration forensics, climate proxy interpretation, and ecohydrology of terrestrial systems. However, the extent to which these patterns can be empirically predicted across Canada and the northern United States has not been fully articulated, in part due to a lack of time series precipitation isotope data for major regions of North America. In this study, we use multiple linear regressions of CNIP, GNIP, and USNIP observations alongside climatological variables, teleconnection indices, and geographic indicators to create empirical models that predict the δ^{18}O of monthly precipitation ($\delta^{18}O_{ppt}$) across Canada and the northern United States. Five regionalization approaches are used to separate the study domain into isotope zones to explore the effect of spatial grouping on model performance. Stepwise regression-derived parameterizations quantified by permutation testing indicate the significance of precipitable water content and latitude as predictor variables. Within the Canadian Arctic and eastern portion of the study domain, models from all regionalizations capture the interannual and intraannual variability of $\delta^{18}O_{ppt}$. The Pacific coast and northwestern portions of the study domain show less agreement between models and poorer model performance, resulting in higher uncertainty in simulations throughout these regions. Long-term annual average $\delta^{18}O_{ppt}$ isoscapes are generated, highlighting the uncertainty in the regionalization approach as it compounds over time. Additionally, monthly time series simulations are presented at various locations, and model structure uncertainty and 90% bootstrapped prediction bounds are detailed for these predictions.

1. Introduction

Precipitation isotopes (δ^{18}O and δ^{2}H) are natural tracers providing diverse attributes for understanding processes characterizing the water cycle at local, regional, and continental scales. This understanding is of paramount importance today as water resources provide the basis of rural and urban community sustainability, commercial industries, and the delivery of essential ecosystem services. While precipitation amounts and patterns are relatively well quantified, it is only over the last 25 years that we have begun to rigorously explore the spatial patterns of water cycle isotopes at the continental and global scales [*Rozanski et al.*, 1993; *Welker*, 2000, 2012; *Dutton et al.*, 2005; *Birks and Edwards*, 2009; *Vachon et al.*, 2010a; *Liu et al.*, 2013]. Woven into these spatial pattern analyses—termed "isoscapes"—is now the ability to resolve processes and mechanisms that may be controlling the temporal variability in water cycle isotopes such as moisture source and climate conditions along the rainout trajectory [*Rozanski et al.*, 1992; *Birks and Edwards*, 2009; *Liu et al.*, 2010; *Vachon et al.*, 2010b; *Welker*, 2012].

Past efforts to predict oxygen-18 and deuterium distributions in precipitation ($\delta^{18}O_{ppt}/\delta^{2}H_{ppt}$) have typically focused on creating isoscapes of long-term annual or seasonal averages at both the global scale [*Birks et al.*, 2002; *Bowen and Wilkinson*, 2002; *Bowen and Revenaugh*, 2003] and regional/continental scale for the United States [*Dutton et al.*, 2005; *Welker*, 2012] and China [*Liu et al.*, 2008] utilizing a coupled regression and geostatistical modeling approach. These initial studies placed high importance on geographical parameters (elevation and latitude) as proxies for more physically based parameters to approximate Rayleigh distillation

(i.e., the amount of temperature-dependent rainout that occurs as an air mass is transported to locations of higher latitude and/or elevation without any secondary processes) [*Dansgaard*, 1964]. More recent studies have begun incorporating climate parameters within the prediction models at the regional scale for Austria [*Liebminger et al*., 2006], the eastern Mediterranean [*Lykoudis and Argiriou*, 2007; *Lykoudis et al*., 2010], China [*Zhao et al*., 2011], Ireland [*Fischer and Baldini*, 2011], and Canada [*Delavau et al*., 2011]; and at the global scale [*Van der Veer et al*., 2009; *Terzer et al*., 2013]. While these approaches have provided useful depictions of long-term annual and seasonal averages for many regions, most of these estimates are not suitable for predicting precipitation isotope compositions on the time scale necessary for many hydrological applications, such as iso-hydrological modeling, where a temporal frequency of monthly time series (or finer) compositions are required for model forcing [*Stadnyk et al*., 2013].

This study focuses on the creation of time series $\delta^{18}O_{ppt}$ predictions at a monthly temporal frequency across Canada and the northern United States. The objectives of this study are to: (1) quantify the degree to which empirical models utilizing climate and geographic parameters capture the variability in monthly time series $\delta^{18}O_{ppt}$ observations across the study domain and, (2) provide an estimate of uncertainty associated with the empirical simulations that reflects the boundaries of expected seasonal variation. Establishing this knowledge is essential for future applications in coupled iso-hydrological modeling, where isoscapes provide the basis for modeling applications (specifically in ungauged or sparsely gauged locations, such as most of northern Canada) and input uncertainty is propagated into hydrological model output.

2. Data and Methods

2.1. Observations and Gridded Products

2.1.1. Oxygen-18 in Precipitation

Oxygen-18 in precipitation is used as the dependent variable for model development in this study. Three data networks provide $\delta^{18}O_{ppt}$ measurements for this research: the Canadian Network for Isotopes in Precipitation (CNIP) [*Birks and Gibson*, 2009], the United States Network for Isotopes in Precipitation (USNIP) [*Welker*, 2000, 2012], and the Global Network for Isotopes in Precipitation (GNIP), coordinated by the International Atomic Energy Agency/World Meteorological Organization (IAEA/WMO) [*Aggarwal et al*., 2011; *International Atomic Energy Agency/World Meteorological Organization*, 2014]. Canadian precipitation samples are collected at a monthly frequency by the CNIP and GNIP networks, with the exception of the supplementary Calgary record which is taken from *Peng et al*. [2004]. Calgary $\delta^{18}O_{ppt}$ observations are obtained from short-term sampling (0.5-3 days) and are amount weighted to monthly compositions for direct comparison to CNIP and GNIP measurements utilizing the following formula:

$$\delta^{18}O_{ppt\ \ monthly} = \sum P_i * (\delta^{18}O_{ppt})_i / \sum P_i \quad (1)$$

P_i is the amount of each individual precipitation sample. Weekly precipitation composites are collected throughout the northern tier of the U.S. at the 27 USNIP sites included in this study [*Welker*, 2000, 2012; *Dutton et al*., 2005; *Vachon et al*., 2007]. Utilizing the precipitation amount-weighting approach outlined in equation (1), weekly USNIP $\delta^{18}O_{ppt}$ compositions are amount weighted to monthly composites utilizing precipitation data obtained from the NTN (National Trends Network) Branch of the NADP (North America Deposition Program) (nadp.sws.uiuc.edu). Figure 1 depicts the temporal distribution of the CNIP/GNIP (stations 1–36) and USNIP (stations 37–63) observations at each station. Figure 2d displays the stations spatially across the study domain. The supporting information for this study summarizes the station name, location, years, and number of monthly measurements at each station.

On average, the CNIP/GNIP and USNIP networks have a similar number of monthly observations per station (CNIP/GNIP: n ~107; USNIP: n ~109). However, USNIP measurements are more uniformly distributed between stations in comparison to CNIP/GNIP measurements, which overall have more variability in their temporal distribution, ranging from n=14 monthly compositions at Inuvik (station 20), to n=331 at Ottawa (station 23) (Figure 1). USNIP observations used in this study consistently begin in 1989 and conclude in 2004; whereas CNIP and GNIP observations are collected between the years of 1961–2010, with minimal consistency in period of record between stations. These temporal and spatial discontinuities in $\delta^{18}O_{ppt}$ records may negatively affect model development, potentially biasing model parameters in data-sparse regions, such as northern Canada and Alaska. Pre-1979 observations are excluded due to the lack of North

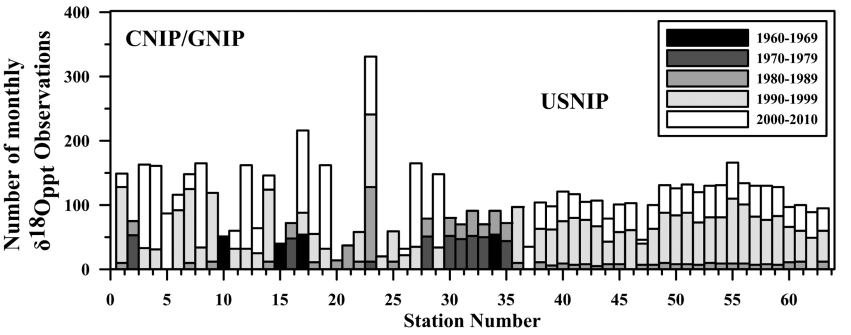

Figure 1. Distribution of CNIP/GNIP and USNIP monthly $\delta^{18}O_{ppt}$ compositions at each station. Number of monthly observations within each decade is specified.

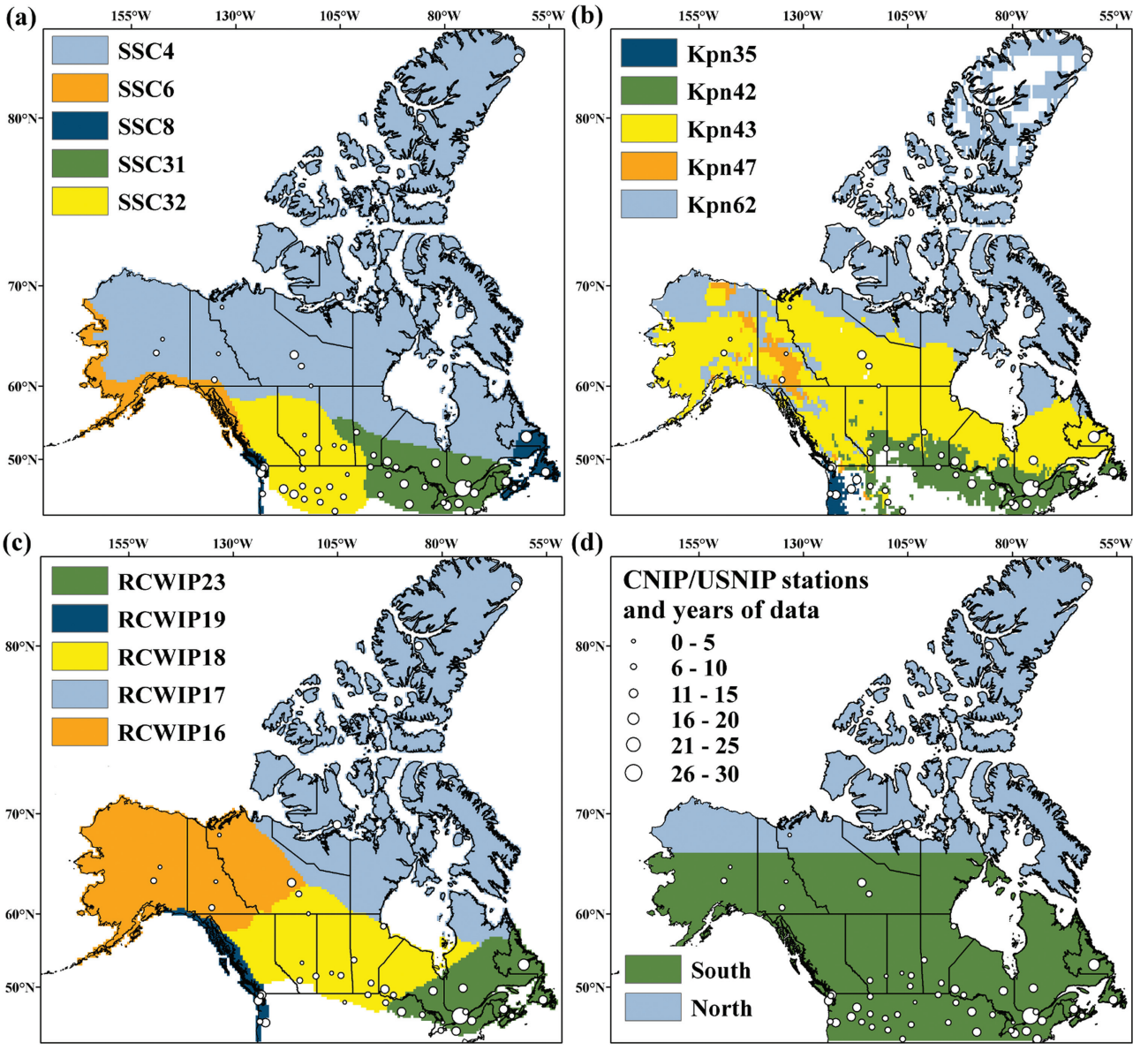

Figure 2. Study domain regionalization into isotope zones: (a) SSC, (b) Kpn, (c) RCWIP, and (d) 2 Zone. The CNIP, GNIP, and USNIP stations included in each zone are indicated, alongside the number of years of data at each station, represented by the magnitude of the symbol.

Table 1. Variables Included in Regression Model Development

Variable ID	Description	Frequency	Source
Climate Variables			
apcp	Accumulated total precipitation	Monthly total	NARR
cape	Convective available potential energy	Monthly average	NARR
cdcon	Mean of convective cloud cover	Monthly average	NARR
cdlyr	Mean of nonconvective cloud cover	Monthly average	NARR
evap	Accumulated total evaporation	Monthly total	NARR
hcdc	High cloud area fraction	Monthly average	NARR
hpbl	Planetary boundary layer height	Monthly average	NARR
mcdc	Mean cloud area fraction	Monthly average	NARR
prwtr	Precipitable water for entire atmosphere	Monthly total	NARR
rhum2m	Relative humidity at 2 m	Monthly average	NARR
uwnd10m	U-wind at 10 m (zonal)	Monthly average	NARR
vwnd10m	V-wind at 10 m (meridional)	Monthly average	NARR
wcconv	Water condensate flux convergence	Monthly average	NARR
wcvflx	Water condensate meridional flux convergence	Monthly average	NARR
Teleconnection Indices			
AMO	Atlantic Multidecadal oscillation	Monthly	NOAA
AO	Arctic oscillation	Monthly	NOAA
NAO	North Atlantic oscillation	Monthly	NOAA
PDO	Pacific decadal oscillation	Monthly	JISAO
PNA	Pacific North American pattern	Monthly	NOAA
SOI	El Nino/La Nina (Southern oscillation index)	Monthly	NOAA
Geographic Variables			
LAT	Latitude	N/A	CNIP/GNIP/USNIP
LONG	Longitude	N/A	CNIP/GNIP/USNIP
ALT	Altitude (elevation)	N/A	CNIP/GNIP/USNIP
Dummy Variables			
SIN	Sine function	Monthly	N/A
COS	Cosine function	Monthly	N/A

American Regional Reanalysis (NARR) climate data, resulting in over 6000 $\delta^{18}O_{ppt}$ observations for use in this modeling study.

2.1.2. Climate and Geographic Data

To approximate $\delta^{18}O_{ppt}$ time series for a region as large and climatically diverse as Canada and the northern United States, parameters with the ability to capture the multitude of factors contributing to $\delta^{18}O_{ppt}$ variability across the study domain need to be incorporated into the modeling framework. The variables included in this approach (Table 1) are selected based on this goal.

The climate data in this study are from the National Centers for Environmental Prediction (NCEP) NARR data set. NARR is a long-term atmospheric and land surface hydrology reanalysis data set spanning the North American domain [*Mesinger et al*., 2006]. NARR utilizes lateral boundary conditions from the NCEP-DOE (Department of Energy) Global Reanalysis and makes use of the data assimilation system from the NCEP Eta Model. This data set is available from 1979 to 2003, and is continued post 2003 as the Regional Climate Data Assimilation system (R-CDAS). NARR has a spatial resolution of 32 km, and utilizes 45 layers in the vertical. For this study, monthly time series of selected climate variables (Table 1) are extracted from the NARR grid cell closest to each CNIP/GNIP or USNIP measurement location. Total precipitation, convective precipitation, total evaporation, and precipitable water variables are converted to monthly totals from monthly averages.

In addition to the 20 NARR climate variables, three geographic indicators and six teleconnection indices are incorporated as potential predictors within the models (Table 1). Teleconnection indices are obtained from the National Oceanic and Atmospheric Administration (NOAA) and University of Washington's Joint Institute for the Study of the Atmosphere and Ocean (JISAO). Finally, sine and cosine curves with one complete cycle per year are used as a smoothing function of time (i.e., "dummy variables") to account for seasonal effects that may not be captured by the aforementioned predictors [*Peng and Dominici*, 2008; *Chun*, 2010].

2.2. Model Regionalization

Pooling information from nearby locations within a region can be useful due to the similarity of processes and mechanisms controlling the variability in $\delta^{18}O_{ppt}$. Given the large geographic area and diverse climate

conditions and moisture sources (e.g., Pacific Ocean, Gulf of Mexico, Arctic, recycled continental moisture) present across northern North America, a single empirical relationship may not be universally applicable throughout the entire study domain. Our hypothesis is that empirical models for predicting monthly time series of precipitation $\delta^{18}O$ may be improved if they are developed specifically for individual "isotope zones." By identifying isotope zones based on well-established meteorological and climatological zones where moisture sources and hydroclimate parameters are likely more similar, we hope to improve our ability to understand the physical parameters controlling isotopic labeling in different regions as well as improve predictions of $\delta^{18}O$ time series. For these reasons, five different regionalization approaches (three of which are based on established classification schemes) are used to separate the study domain into isotope zones to explore the effect of regionalization on model performance and to investigate the outcome of regionalization on model structure uncertainty (i.e., selection of model parameters). Isotope zones are displayed on Figure 2, whereby $\delta^{18}O_{ppt}$ observations from stations within the boundaries of each zone are used to create a set of seasonal empirical models for that specific zone.

The Synoptic Scale Classification (SSC) [*Kalkstein et al*., 1996; *Sheridan*, 2002] (S. Sheridan, available at http://sheridan.geog.kent.edu/ssc.html) system is a hybrid system, and therefore uses both manual and automated methods to classify daily weather conditions into one of six different weather types, or a transition between weather types, at a station by station basis across the North American continent. Classification is solely based on surface observations at individual stations (including temperature, dew point, wind, pressure, and cloud cover). Since the SSC does not incorporate any upper level conditions or air mass source, the SSC is primarily a weather-type classification system and not an air mass classification system. SSC climate zones are created based on principal component analysis (PCA) decomposition of seasonal normals and a k-means cluster analysis. Canada is separated into five zones, Arctic (SSC4), Boreal Coast (SSC6), Marine (SSC8), Laurentian (SSC3a- herein referred to as SSC31), and Northern Rockies (SSC3b—herein referred to as SSC32) (Figure 2a).

The Köppen-Geiger (Kpn) climate classification system is the most commonly used global climate classification. The historical world map of Köppen-Geiger climate classes was recently updated utilizing global data sets of monthly temperature and precipitation observations covering the 50 year period of 1951–2000 [*Kottek et al*., 2006]. The Köppen-Geiger classification labels zones across the globe by a three letter name, indicating the main climate, precipitation type, and air temperature, respectively. Ten Köppen-Geiger climate zones exist within Canada, whereby CNIP stations are situated within five of these zones representing approximately 97% of the Canadian land mass (Figure 2b): Kpn35 (Csb—warm temperate, steppe precipitation, warm summer), Kpn42 (Dfb—snow, fully humid precipitation, warm summer), Kpn43 (Dfc—snow, fully humid precipitation, cool summer), Kpn47 (Dsc—snow, steppe precipitation, cool summer), and Kpn62 (ET-polar tundra).

The third classification system is the Regionalized Climatic Water Isotope Prediction (RCWIP) approach [*Terzer et al*., 2013]. RCWIP utilizes weighted fuzzy clustering techniques (including fuzzy c-means) to build climate clusters from Global Historical Climate Network (GHCN) records, incorporating normalized climatic variables of monthly mean temperature and precipitation and spatial variables (latitude and longitude), resulting in 36 climatic clusters across the globe. Six of the 36 clusters encompass the Canadian domain, with CNIP stations located within five of the six: RCWIP16 (Dfc), RCWIP17 (ET), RCWIP18 (Dfb), RCWIP19 (Cfb—warm temperate, fully humid precipitation, warm summer), and RCWIP23 (Dfb) (Figure 2c). Our approach utilizes the CNIP, GNIP, and USNIP measurements within the aforementioned five climate clusters, resulting in an enhanced data set used for the current regionalization relative to the RCWIP study.

The final two classification systems represent more simplified regionalization approaches. The 2 Zone classification scheme separates the study domain into north and south zones, with the border between zones located at the Arctic Circle (Figure 2d). The 1 Zone regionalization (not shown) is the most simplistic approach, whereby no regionalization occurs, and all available $\delta^{18}O_{ppt}$ data are utilized in model development, excluding those set aside for validation purposes.

2.3. Regression Model Development

The general approach to developing regression models capable of predicting time series of $\delta^{18}O$ for each of the regionalization schemes includes a statistical evaluation of which parameters to include, an examination

of the regression diagnostics to assess model deficiencies (e.g., collinearity, autocorrelation, etc.) and quantification of the model uncertainty.

A multiple linear regression approach is utilized to create the empirical models in this study. The general expression of the ordinary least squares (OLS) regression model of precipitation oxygen-18 compositions is:

$$\delta^{18}O_{ppt} = X\beta + \varepsilon \quad (2)$$

X is a matrix of regression variables which can be NARR climate variables, geographical variables, or teleconnection indices, β is the regression coefficient array, and ε represents the regression residuals. Prior to model creation, the relationship between potential predictors (Table 1) and $\delta^{18}O_{ppt}$ is assessed through OLS regression, and variables are natural-log transformed if necessary to linearize relationships. Additionally, data are standardized to assist with numerical stability. Seasonal models are created for each zone within the five regionalizations. A season is defined as: winter, December–January–February (DJF); spring, March–April–May (MAM); summer, June–July–August (JJA); and fall, September–October–November (SON). The SSC6 and Kpn47 isotope zones only include 34 and 69 observations for model calibration, respectively. For this reason, annual models are utilized within these zones to ensure adequate data for model development. This methodology results in a total of 66 empirical models for evaluation. A split sample calibration and validation modeling approach is utilized, whereby a portion of the $\delta^{18}O_{ppt}$ observations are removed from the data set to serve as a separate validation data set. Based on spatial and temporal data availability, the years 1982, 1985, and 2000 are selected to serve as a portion of the validation subset. Using three random discrete years instead of three consecutive years can help to alleviate the autocorrelation problem due to low-frequency oscillations (e.g., PDO) which cause decadal dry or wet periods. Using a consecutive period (either dry or wet) for validation or calibration will introduce bias into our parameters. The remainder of the validation data set comprises four additional USNIP stations from the various isotope zones (station numbers 37, 47, 52, and 55), resulting in approximately 14.3% of the $\delta^{18}O_{ppt}$ observations for validation and 85.7% for calibration, on average. The regression models utilize all $\delta^{18}O_{ppt}$ observations within a specified zone as either calibration or validation data for model development. The amount of measurements for calibration and validation within each model is provided in the supporting information.

2.3.1. Parameter Selection

Selection of the climate variables, teleconnection indices, and geographical parameters to include in each of the models is made using a stepwise regression approach in Matlab software [*The MathWorks Inc*., 2013]. This approach utilizes forward and backward stepwise regression to add or remove predictor variables from the regression models. The advantage of this method is that it allows flexibility in selecting the criterion and threshold to add or remove terms from the model. The Akaike Information Criteria (AIC) [*Akaike*, 1974] is used for this application, and is defined as:

$$AIC_i = -2\log(L_i) + 2(V_i) \quad (3)$$

L_i is the log likelihood for model i, with V_i free parameters. Smaller values of the AIC indicate a better model fit. Addition of parameters to the model is an iterative procedure by changing the AIC threshold, and assessing if the retained parameters are statistically significant and free of multicollinearity issues. Statistical significance is assessed by permutation tests [*Good*, 2005] conducted in the R-software lmPerm package [*Wheeler*, 2010], the results of which are used as a guide to remove insignificant parameters. Permutation tests are selected as they are nonparametric and therefore make no assumptions of the underlying distribution of the model residuals. It should be noted that quadratic terms and interaction between terms are considered within the models included in this study.

2.3.2. Regression Diagnostics

Regression diagnostics are used to evaluate whether the assumptions regarding the dependent and independent variables and modelled residuals are valid, and to diagnose model deficiencies. The presence of multicollinearity is assessed through calculation of Variance Inflation Factors (VIFs). VIFs greater than five suggest that multicollinearity is present and are further investigated. Normally distributed model residuals are required to satisfy model assumptions, specifically with respect to hypothesis testing and calculation of confidence intervals for slope coefficients or prediction intervals for individual $\delta^{18}O_{ppt}$. Although we have taken steps to utilize nonparametric approaches, normality is still assessed qualitatively through box plots

or quantile-quantile (QQ) plots of the residuals, alongside utilization of the Lilliefors test for normality [*Lilliefors*, 1967]. Homoskedasticity is graphically evaluated through plots of residuals versus predicted $\delta^{18}O_{ppt}$.

Another assumption of OLS regression is independence of the residuals. Provided that we are working with spatiotemporal data, this assumption is thoroughly examined. To investigate if the models display serial correlation, the autocorrelation function (ACF) is calculated for lag values from 0 to 20 and tested against standard-error bands for white noise at each sampling station. Additionally, plots of model residuals versus time are examined at each measurement location, and the Durbin-Watson statistic [*Durbin* and *Watson*, 1951] is calculated and compared with published Durbin-Watson significance tables as a check. The second aspect of independence involves assessing the existence of spatial correlation. Semivariograms of model residuals (not shown) are plotted to identify the critical distance that is influenced by spatial correlations. Overall, we do not see significant spatial or temporal correlation in model residuals. The distances between stations are generally larger than the decorrelation distance.

2.3.3. Uncertainty Quantification

For time-series simulations, a bootstrapping approach [*Davison and Hinkley*, 1997] is utilized to quantify uncertainty of model predictions. Ninety percent prediction intervals are created by estimating the distribution of the prediction error:

$$\delta^* = x_+^T \hat{\beta}^* - (x_+^T \hat{\beta} + \varepsilon_+^T) \tag{4}$$

x_+^T is the explanatory variable matrix, $\hat{\beta}^*$ is the simulated vector of parameter estimates from the model-based resampling algorithm, $\hat{\beta}$ is the ordinary least squares estimates of the parameter vector, and ε_+^T is the vector of prediction errors from the resampled model, which are sampled from $\hat{G}$, the empirical distribution function of the centered modified residuals, $r_i - \bar{r}$. Modified residuals are calculated as follows:

$$r_i = e_i/(1-h_i)^{1/2} \tag{5}$$

e_i are the raw residuals form the regression model and h_i are the respective leverages. The exact quantiles are estimated by sampling the empirical quantiles of ranked δ*s. This estimated distribution is generated from 1000 iterations of the resampling algorithm for each point in time and space where a prediction is required. This approach is applied to each of the five regionalization schemes, and the uncertainty due to model structure (i.e., method of regionalization) is also quantified.

3. Results and Discussion

3.1. Model Performance, Parameterization, and Diagnostics

Results are summarized for the 66 models created within this study and are outlined in the following section. Figure 3 shows the average number of parameters retained within each zone, and provides a seasonal analysis of significant parameters for the prediction of $\delta^{18}O_{ppt}$. "Combined" box and whisker plots of the model residuals (Figure 4) display model performance within each zone. Additionally, due to the differing number of observations incorporated within each model, performance for each regionalization scheme is evaluated station by station through the mean squared error (MSE), residual excess kurtosis, and residual inter quartile range (IQR) (Figure 5) to more directly compare model results.

The combined box and whisker plots on Figure 4 display the calibration (Figure 4a) and validation (Figure 4b) residuals from all seasons for each zone within a regionalization. Residuals greater than 1.5*IQR are classified as possible outliers (hollow diamond symbols), and residuals greater than 3.0*IQR are classified as outliers (red filled diamond symbols). The IQR for each regionalization is indicated to the direct right of each box.

Stepwise regression derived parameterizations (Figure 3a) indicate the importance of several variables that repeatedly survive the selection procedure. The most frequently retained climate predictor variable is precipitable water content, followed by mean cloud area fraction, evaporation, and water condensate meridional flux convergence. Although not temporally variant, geographic parameters explain enough variance in monthly time series $\delta^{18}O_{ppt}$ to be retained in a large portion of the empirical models, specifically the latitude and longitude predictors. Latitude and precipitable water account for the largest components of the variance in simulated $\delta^{18}O_{ppt}$, which is not surprising, since many of the "effects" described by *Dansgaard*,

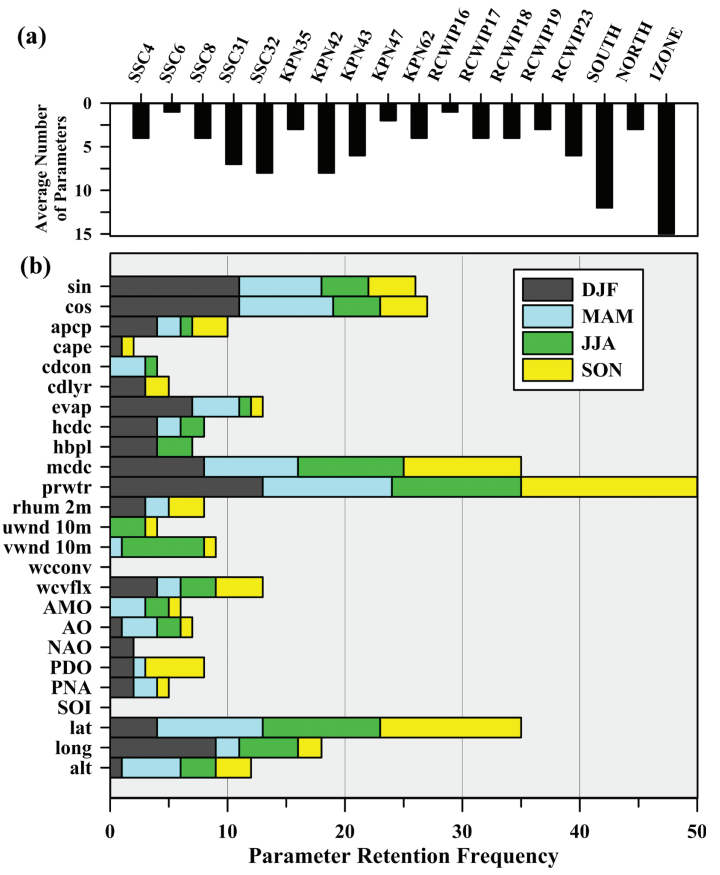

Figure 3. (a) Average number of parameters retained within each model, and (b) overall seasonal parameter retention frequency for all models.

[1964] (e.g., temperature effect, altitude effect, continental effect) are derived from the amount of precipitable water present in an air mass. Other studies have also found strong linkages between $\delta^{18}O_{ppt}$ and precipitable water content [e.g., *Dansgaard*, 1964; *Araguás-Araguás et al*., 2000] and atmospheric moisture residence time [*Aggarwal et al*., 2012]. This relationship between precipitable water content and $\delta^{18}O_{ppt}$ appears to strengthen in high latitude regions (i.e., SSC4, KPN62, RCWIP17, and NORTH models) as this variable is retained in 100 percent of northern models (16/16), while the number of other parameters remains relatively low (on average, less than three additional parameters per model in this region).

The prediction of $\delta^{18}O_{ppt}$ becomes increasingly complex within lower latitude continental zones, where the correlation with precipitable water is still prominent, however, is confounded by additional effects, such as recycling of water from evaporating Great Lakes [*Gat et al*., 1994], and transpiration of meteoric water from soils into the atmosphere [*Yakir and Sternberg*, 2000], resulting in an increased variety and number of parameters retained in the models within these central Canadian/U.S. regions (SSC31/32, KPN42/43, RCWIP23, and SOUTH models). Although model parameterizations become increasingly complex in these regions, overall model performance within the southeastern region (SSC31, Kpn42, and RCWIP23) is consistently strong, with relatively low IQR compared to other zones (ranging from 2.63 to 3.07). South-central and western regions (SSC32, Kpn43, RCWIP18) also display a high parameter retention rate (on average, six parameters retained per model), however, show relatively poorer simulation statistics (IQR's range from 3.50 to 3.71), potentially indicating more complex isotope-climate relations within these regions. Both low-latitude coastal zones (SSC8, Kpn35, RCWIP19) and northwestern regional models (SSC6, KPN47, RCWIP16) typically show poor correlation between $\delta^{18}O_{ppt}$ and predictor variables, resulting in very low parameter retention rates (on average, less than three parameters retained per model). This lack of correlation is likely associated with the low seasonality of precipitation isotopes in coastal regions in general [*Welker*, 2000; *Vachon et al*., 2007] and changes in oceanic source [*Fisher et al*., 2004]. The isotopic labeling of precipitation in paleorecords from the northwestern region has been attributed to changes in oceanic source rather than local climate parameters [*Fisher et al*., 2004], therefore the poor correlation between $\delta^{18}O_{ppt}$ and local climate parameters is not surprising. Although IQR's are low in this region (ranging from 2.62 to 2.85) and outliers are less prevalent than other models, this is likely due to subdued seasonality in these locations rather than superior model performance.

Overall, the 1 Zone and 2 Zone models show relatively comparable yet slightly higher IQR's (ranging from 3.39 to 3.50). Models from these more simplistic regionalizations are more outlier-prone, resulting in an increased occurrence of high-magnitude outliers in comparison to the rest of the models. It should also be

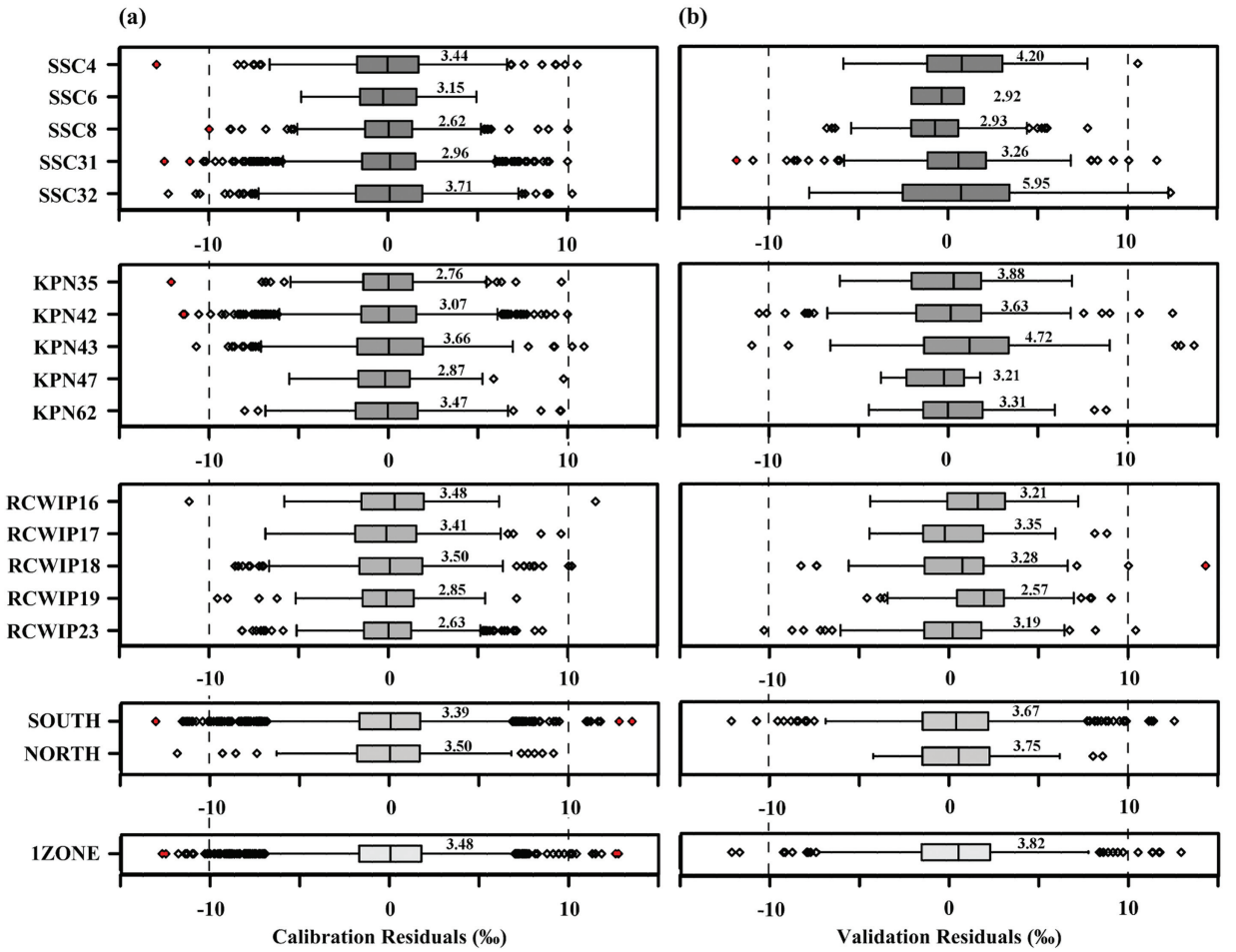

Figure 4. Residual box and whisker plots for the (a) calibration and (b) validation subsets of each regionalization.

noted that reducing the number of zones within a regionalization results in an increased parameter retention rate and therefore more complex, less parsimonious models overall.

Teleconnection indices are retained in 35 percent of all models, therefore demonstrating moderate correlation with monthly time series $\delta^{18}O_{ppt}$ for this type of modeling application. PDO and PNA are most typically retained during the fall and winter seasons in the west and central zone models (e.g., SSC31/32, Kpn 42/43, RCWIP18/19, etc.), while NAO is included in two central region models (SSC32 and Kpn43) during the winter season. The majority of the models incorporating the AO index are for northern regions (SSC4, Kpn62, RCWIP16/17, etc.), typically during MAM; however, retention of AO throughout all seasons is present. The aforementioned indices have been established to have significant relationships with cold season precipitation, primarily for the west and central (PDO), and within the province of Alberta (PNA), and northeastern regions of Canada (NAO/AO) [*Bonsal* et al., 2001; *Bonsal and Shabbar*, 2011]. Strong correlations have been found between the PNA index and the $\delta^{18}O$ of precipitation in the Canadian prairies [*Birks and Edwards*, 2009]. The AMO index is retained during warmer seasons (MAM, JJA and SON) throughout the south-central models (SSC31/32, Kpn43, etc.). *Bonsal and Lawford* [1999] indicate that the positive phase of AMO is related to dry summer conditions over the central and northern regions of the Canadian Prairies and the lower Great Lakes and St. Lawrence Valley. This agreement between the timing and location of retained teleconnection indices and the aforementioned studies suggests the teleconnection predictors make physical sense.

To further diagnose spatial and temporal bias or deficiencies in the models, residuals from the five regionalization schemes are grouped by station, and the MSE is examined on a seasonal basis (Figure 5). To assist

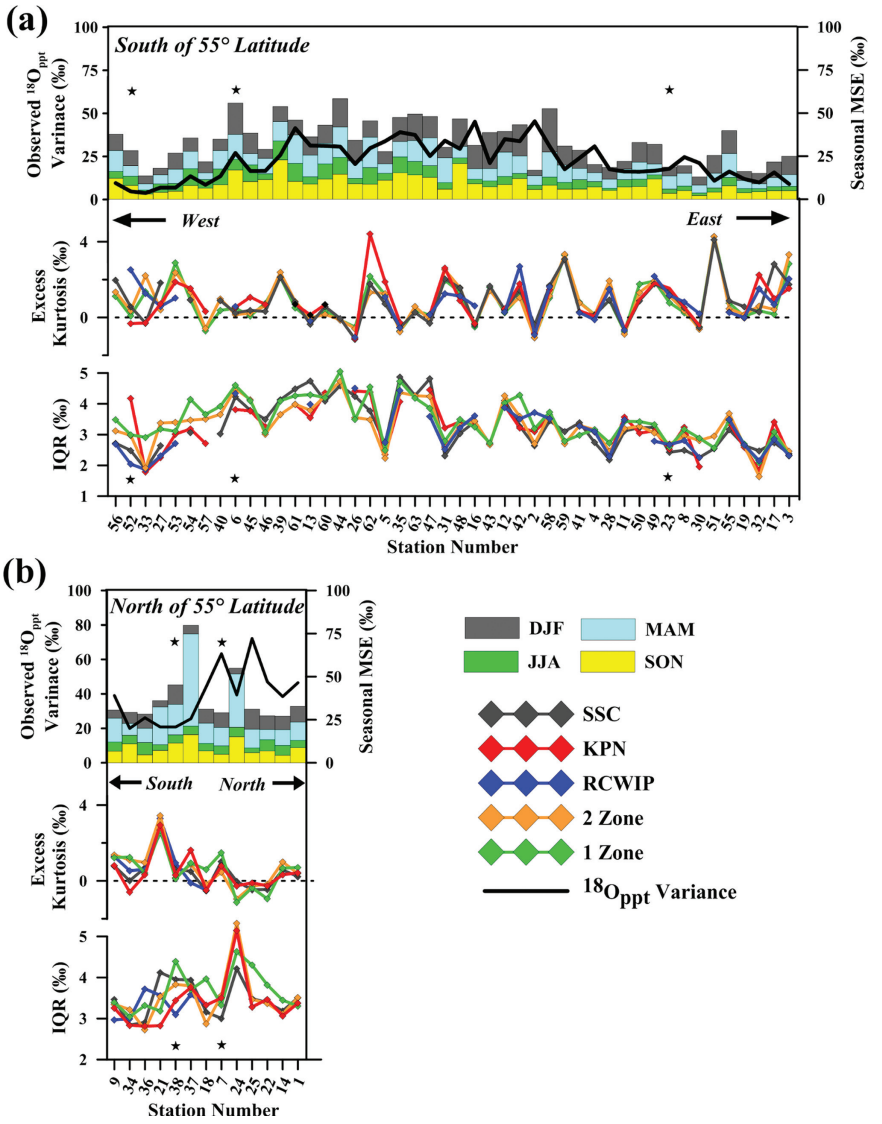

Figure 5. Seasonal MSE (bar chart), for all model residuals at each station, and excess kurtosis and IQR's for individual regionalizations (scatter plots) at each station. Stations are grouped into two subsets: (a) stations located south of 55° latitude, ordered from west to east; (b) stations located north of 55° latitude, ordered some south to north. Variance in observed $\delta^{18}O_{ppt}$ is indicated by the black line. Star symbols indicate stations displayed in further detail below on Figure 6.

with spatial analyses, stations are classified as either north or south of 55° latitude. Southerly stations are ordered by longitude and displayed from west to east, and northern stations are sorted by latitude, with the northernmost stations (station numbers 18–1) located coastally on the Arctic Archipelago. In an attempt to differentiate model performance spatially, residual IQR and excess kurtosis between observed and simulated $\delta^{18}O_{ppt}$ for each regionalization are plotted alongside MSE.

The first item of mention from Figure 5 is that overall, the 1 Zone and 2 Zone simulations show higher IQRs and higher magnitude kurtosis effects than the SSC, Kpn, and RCWIP simulations, supporting findings from the box and whisker plots (Figure 4). Spatially, the smallest residual IQRs (and lowest MSE) generally occur at southerly located coastal stations (both Pacific and Atlantic) and stations throughout southeast Canada and U.S. (Figure 5a). These are typically locations where the variability in $\delta^{18}O_{ppt}$ observations is considered average or below average. *Vachon et al.* [2007] noted that although $\delta^{18}O_{ppt}$ variability is moderate within the Great Lakes, Ohio River Valley, and Northeast regions, very little interannual variability in seasonal precipitation is observed. This consistency from year to year may lead to strong model performance at these locations. Regions of larger residual IQR's (and higher MSE) are located in both the south (below 55°

latitude) and north (above 55° latitude) continental Canada and U.S., particularly the west and central regions. In many instances, these are at locations of higher altitude and display above average variance in observed $\delta^{18}O_{ppt}$. These attributes may, in part, be driven by the stronger intraannual variance in $\delta^{18}O_{ppt}$ values for colder continental regions, such as the high-altitude sites of the Alps and the Rocky Mountains and the deep interior of the UAS in Nebraska and Wisconsin [*Rozanski et al*., 1992; *Harvey and Welker*, 2000; *Welker*, 2000; *Vachon et al*., 2007]. Correlation coefficients (*r*) between residual IQR and observed $\delta^{18}O_{ppt}$ variance, and IQR and altitude are 0.50 and 0.45, respectively (significantly different than zero at the 0.05 level), validating the presence of such trends.

Focusing on high-latitude stations (Figure 5b; latitude $\geq 55°$), there is a larger range in model performance in the more southerly continental stations (stations 9–20), while coastal stations situated within the Arctic Archipelago (stations 18–1) show consistently low error variance despite the large variability in observed $\delta^{18}O_{ppt}$, with the exception of station 24, Pond Inlet. This is primarily attributed to the small number of observations at this station (n=20), whereby the few larger magnitude residuals occurring in MAM and SON skew the MSE. The northern models seem to be able to capture the annual cycle in observed $\delta^{18}O_{ppt}$, further reinforcing a strong correlation with precipitable water and potentially fewer complicating factors influencing Rayleigh distillation in this region.

Temporally, the least amount of error occurs during the summer (JJA) season (this is consistently the case for almost all stations throughout the study domain). In many instances, the largest errors occur during the cold season in winter (DJF) and spring (MAM). However, this trend is less consistent and varies spatially across the domain. For instance, southwest continental stations (e.g., station numbers 54, 57, 40, 45, 46, 39, etc.) show increased warm season (JJA and SON) contributions to error variance. These temporal trends in the distribution of error may be related to the increased contributions of recycled moisture during the warmer months, potentially acting to dampen the portion of variability in $\delta^{18}O_{ppt}$ related to air mass circulation and trajectory. The parameters utilized in the models cannot diagnose changes in moisture trajectory or source, therefore resulting in increased error at locations and times of year when these effects are most prominent on the composition of $\delta^{18}O_{ppt}$.

3.2. Time-Series Ensemble Simulations

Five stations from different physiographic zones across the study domain are selected to further investigate seasonal error patterns and to visually quantify the uncertainty in model simulations over time. Bootstrap-generated prediction intervals for each regionalization are produced, and the minimum and maximum prediction bounds alongside model simulations and observed $\delta^{18}O_{ppt}$ are displayed below on Figure 6. To adequately visualize model performance, a 10 year subset of the 34 year (1979–2012) simulation is plotted.

Generally the models are able to capture the timing and magnitude of the intraannual (seasonal) $\delta^{18}O_{ppt}$ cycle, whereby simulations show moderate interannual variation when climate parameters are included within the models. However, the time series plots reveal that although many of the models do quite well predicting monthly $\delta^{18}O_{ppt}$ compositions, showing small to moderate departures from the long-term monthly mean of a given location, they often fail to capture the anomalies in observed $\delta^{18}O_{ppt}$—both enriched and depleted. This suggests that the climatic and geographic variables used in this study, or the modeling methodology itself, are not able to fully describe the complex physical processes driving the extreme shifts in $\delta^{18}O_{ppt}$, whether that be a change in moisture source, mixing of air masses, water recycling, secondary effects (such as below-cloud evaporation), or a combination thereof. An example of this is at station 6 (Calgary, Canada), where $\delta^{18}O_{ppt}$ derived from warm weather small rainfall events ($<$4 mm) is known to be affected by partial evaporation of raindrops beneath the cloud base (i.e., secondary evaporation), causing an enrichment in $\delta^{18}O_{ppt}$ under these circumstances [*Peng et al*., 2004, 2007]. There are multiple instances where the models are likely not able to capture this effect and large positive residuals occur during the warmer months.

Many of the results described earlier are also reinforced within the time series plots on Figure 6. For example, station 52 (Alsea Guard Ranger Station) located within the Coast Range Mountains in Oregon, U.S., is a validation station that shows considerable differences between model simulations. As previously mentioned, there is a lack of seasonality in this region and poor correlation between $\delta^{18}O_{ppt}$ and the predictor variables, resulting in a lack of physical basis, poor performance outside the region of calibration, and wider prediction bounds. Simulations in the southeast region of the study domain are quite strong, which can be seen in the time series plot of station 23 (Ottawa, Canada). All ensemble members show very similar results

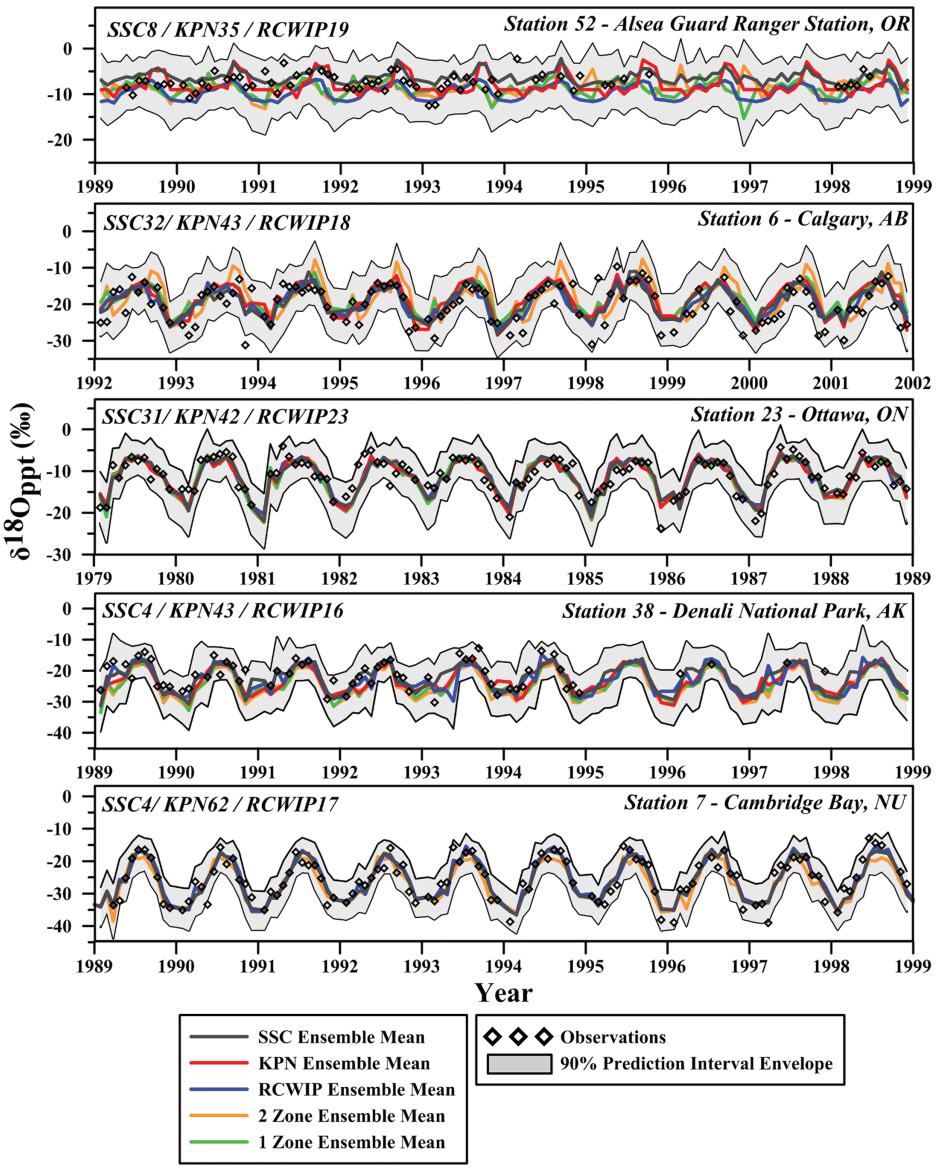

Figure 6. Ten year monthly time series simulations for five stations throughout the study domain. Ensemble means are indicated by the solid lines. $\delta^{18}O_{ppt}$ observations are denoted as black diamonds. The gray-shaded region represents the envelope of bootstrapped 90% prediction intervals for all regionalizations.

throughout this region, resulting in narrow prediction bounds and tightly constrained mean ensemble members. The Arctic Archipelago station models perform comparably well, represented by the time series plot at station 7 (Cambridge Bay, Canada).

3.3. Long-Term Spatial Mapping

Long-term annual average maps of $\delta^{18}O_{ppt}$ across Canada and the northern portion of the U.S. are created for each regionalization, generated from the mean of monthly time series ensembles over the period of 1981–2010. Time series simulations are generated at the grid scale at a resolution of 17 arc minutes and are precipitation amount weighted to create the long-term annual average compositions displayed on Figure 7. The gridded range between the five long-term simulations is displayed to provide an estimate of the model structure uncertainty as it compounds over the aforementioned 30 year period (Figure 7f).

Generally the different models are able to produce long-term annual average $\delta^{18}O_{ppt}$ contours of reasonable magnitude while capturing the main trends in the variability in $\delta^{18}O_{ppt}$, such as depletion from: south to

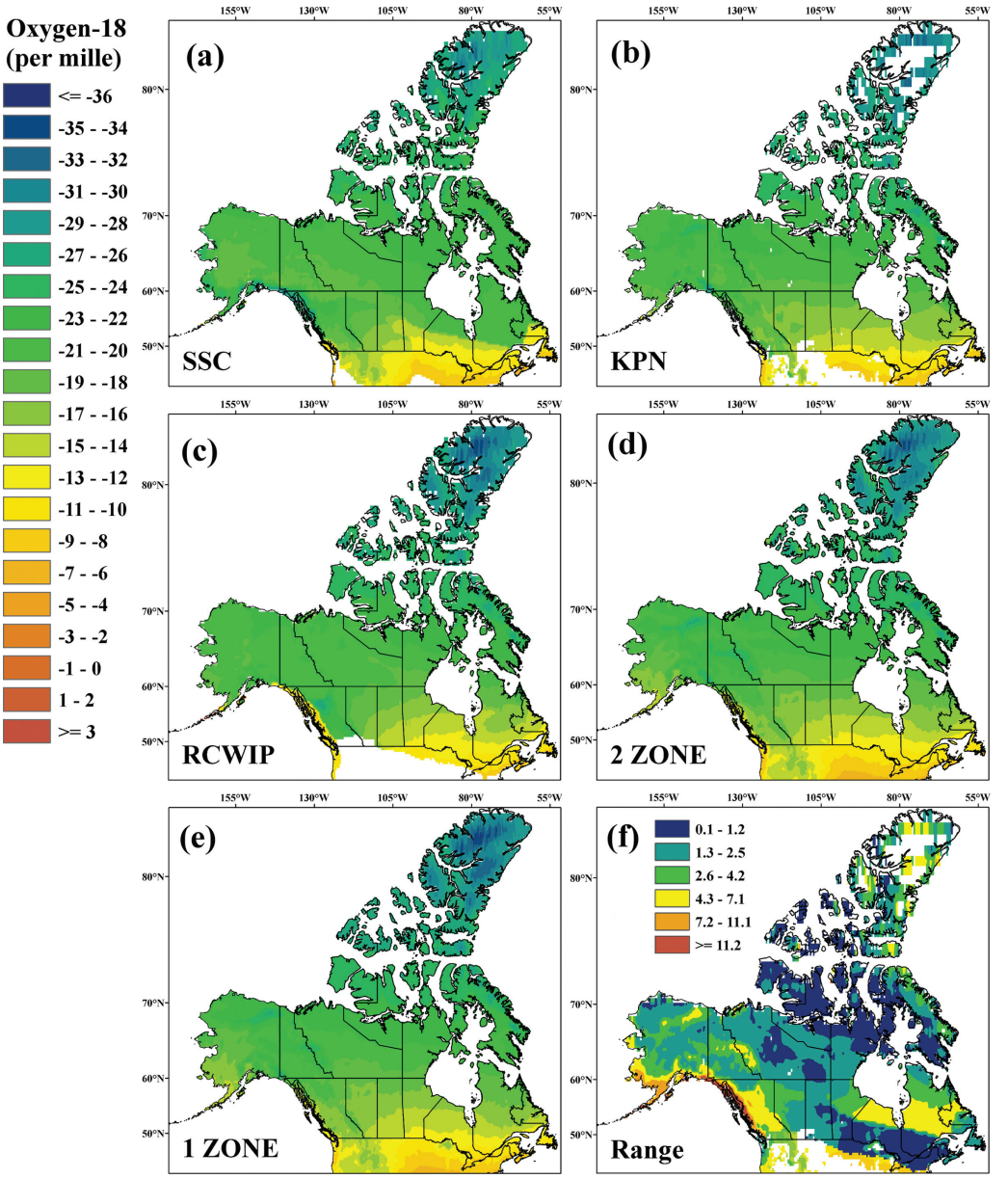

Figure 7. Long-term precipitation amount weighted annual average $\delta^{18}O_{ppt}$ simulations (units of ‰) for: (a) SSC, (b) Kpn, (c) RCWIP, (d) 2 Zone, and (e) 1 Zone regionalizations. The gridded range in long-term simulations is displayed on Figure 7f.

north (latitude effect), coast to interior (continentality), and in areas of high elevation (altitude effect) [*Dansgaard*, 1964]. However, as evident on Figure 7, the SSC and RCWIP regionalizations produce unrealistic border effects at several of the isotope zone boundaries, manifesting in an unrealistic enrichment along west coast of British Columbia and into Alaska (RCWIP) and an extremely sharp transition from relatively depleted to enriched in heavy isotopes within the northern Ontario, Quebec, and Newfoundland and Labrador region (SSC). The Kpn, 2 Zone and 1 Zone regionalizations appear to have much less apparent border effects due to the nature of the isotope zone locations.

Figure 7f provides an estimate of the long-term uncertainty between the regionalizations. The largest range in model simulations occurs along the Pacific coastal regions of British Columbia and Alaska, while more moderate discrepancies are within the Cordilleran region in British Columbia and Alberta, the western portion of the Mackenzie District in the Northwest Territories and the Yukon Territory, and into Quebec, Newfoundland and Labrador. Regions of model disagreement are caused by either one of two phenomenon:

(1) significant differences in model structure (i.e., parameterization) and therefore discrepancies in model simulations (e.g., southern Pacific Coast models), or (2) similarity in model simulations at locations of model development, but unrealistically placed isotope border locations (e.g., SSC31, SSC6).

Throughout the mid-Arctic, central, and southeastern portions of the study domain, all regionalizations are relatively comparable, resulting in a smaller range in long-term simulations and less uncertainty associated with model structure. The SSC models produce relatively enriched predictions in the Arctic Archipelago in comparison to the remaining four regionalizations, and are the cause of the larger range in model simulations within this region.

4. Conclusions

This study investigates the use of physically based hydroclimate parameters alongside geographic variables and teleconnection indices within an empirical modeling framework to capture the time series monthly variability in observed $\delta^{18}O_{ppt}$. Additionally, the uncertainty due to regionalization is assessed for both time series and long-term average predictions.

Precipitable water content and latitude are found to be the most significant parameters for the time series prediction of $\delta^{18}O_{ppt}$, typically explaining the largest portions of variance in observed $\delta^{18}O_{ppt}$. Within the mid-Arctic to high-Arctic and eastern portion of the study domain, all five regionalizations generate models with the ability to capture the interannual and intraannual variability of $\delta^{18}O_{ppt}$. However, other areas such as the Pacific coast and northwestern portion of the study domain show less agreement between models and poorer model performance, resulting in higher uncertainty in simulations throughout these regions. Overall, the current study is an improvement from the regional simulations reported by *Delavau et al.* [2011] and previous global simulations due to the refined spatial and temporal scales of prediction (i.e., time series versus long-term averages), enhancement of the suite of physically based predictor variables, and the incorporation of uncertainty associated with model predictions.

As previously discussed, results indicate that with long-term predictions, model structure uncertainty can be substantial in certain locations. However, at the monthly time series scale, 90% bootstrapped prediction intervals show that uncertainty of an individual estimate is much greater than that attributed to model structure. Based on these findings, it is our recommendation that future studies continue to incorporate the corresponding method of uncertainty quantification depending upon the temporal scale of predictions required. Uncertainty can be further reduced by continued $\delta^{18}O_{ppt}$ monitoring and through enhancement of existing monitoring networks, particularity in data-sparse regions with high model uncertainty.

In an attempt to reduce border effects, more simplistic regionalizations (2 Zone and 1 Zone) are investigated within the current study. Although border effects are eliminated, these more simplistic regionalizations result in poorer model performance, including higher IQRs and more frequent outliers. SSC, Kpn, and RCWIP simulations perform comparably at most locations of model development. However, it is the extrapolation of the models across the study domain that in many instances causes the major discrepancies between regionalizations. As previously outlined, both the SSC and RCWIP regionalizations produce long-term average maps with unrealistic $\delta^{18}O_{ppt}$ contours. For these reasons, the Kpn regionalization is selected as the preferred regionalization scheme for future iso-hydrologic modeling applications.

The next step in this research is to generate $\delta^{18}O_{ppt}$ monthly time series and the corresponding prediction bounds within the Fort Simpson Basin, NWT, Canada. These simulations will be utilized to force the existing isoWATFLOOD model and create predictions of oxygen-18 in streamflow at this location. Results will be compared to previous simulations in the FSB that were derived from annual average $\delta^{18}O_{ppt}$ model forcing [*Stadnyk et al.*, 2013]. This methodology allows for an assessment of uncertainty relating to model input data (i.e., simulated $\delta^{18}O_{ppt}$ time series) and the resulting uncertainty on simulations of $\delta^{18}O$ in streamflow.

Acknowledgments

CNIP is made possible through the help of the Canadian Air and Precipitation Monitoring Network (CAPMoN) for sample collection—Kaz Higuchi and Dave MacTavish in particular, the Environmental Isotope Laboratory at the University of Waterloo for sample analysis, and Tom Edwards for initiating and maintaining the network. USNIP is supported in part by NSF awards (ESH-0080952, DBI-0923571) to J.M. Welker and is a collaboration with the U.S. National Atmospheric Deposition Network. We would like to thank the IAEA/WMO for the collection, organization, and provision of the GNIP observations utilized in this study. GNIP data are publically available and can be accessed through the WISER database at: http://www-naweb.iaea.org/napc/ih/IHS_resources_gnip.html. Finally, we would like to acknowledge the contributions of our reviewers whose valuable input has improved this manuscript significantly. This research was partially funded by Natural Sciences and Engineering Research Council (NSERC) Alexander Graham Bell Canada Graduate Scholarship (CGS-D).

References

Aggarwal, P. K., K. Froehlich, and R. Gonfiantini (2011), Contributions of the international atomic energy agency to the development and practice of isotope hydrology, *Hydrogeol. J.*, *19*(1), 5–8, doi:10.1007/s10040-010-0648-3.

Aggarwal, P. K., O. A. Alduchov, K. O. Froehlich, L. J. Araguas-Araguas, N. C. Sturchio, and N. Kurita (2012), Stable isotopes in global precipitation: A unified interpretation based on atmospheric moisture residence time, *Geophys. Res. Lett.*, *39*, L11705, doi:10.1029/2012GL051937.

Akaike, H. (1974), A new look at the statistical model identification, *IEEE Trans. Autom. Control*, *19*(6), 716–723.
Araguás-Araguás, L., K. Froehlich, and K. Rozanski (2000), Deuterium and oxygen-18 isotope composition of precipitation and atmospheric moisture, *Hydrol. Processes*, *14*, 1341–1355, doi:10.1002/1099-1085(20000615)14:8<1341::AID-HYP983>3.0.CO;2-Z.
Birks, S. J., and T. W. D. Edwards (2009), Atmospheric circulation controls on precipitation isotope-climate relations in western Canada, *Tellus Ser. B*, *61B*(3), 566–576, doi:10.1111/j.1600-0889.2009.00423.x.
Birks, S. J., and J. J. Gibson (2009), Isotope hydrology research in Canada, 2003–2007, *Can. Water Resour. J.*, *34*(2), 163–176, doi:10.4296/cwrj3402163.
Birks, S. J., J. J. Gibson, L. Gourcy, P. K. Aggarwal, and T. W. D. Edwards (2002), Maps and animations offer new opportunities for studying the global water cycle, *Eos Trans. AGU*, *83*(37), 406, doi:10.1029/2002EO000298.
Bonsal, B. R., and R. G. Lawford (1999), Teleconnections between El Niño and La Niña events and summer extended dry spells on the Canadian Prairies, *Int. J. Climatol.*, *19*, 1445–1458, doi:10.1002/(SICI)1097-0088(19991115)19:13<1445::AID-JOC431>3.0.CO;2–7.
Bonsal B. R., and A. Shabbar (2011), Large-scale climate oscillations influencing Canada, 1900–2008, in *Canadian Biodiversity: Ecosystem Status and Trends 2010, Tech. Thematic Rep. 4*, Can. Counc. of Resour. Minist., 15 pp., Ottawa, Ont. [Available at http://www.biodivcanada.ca/default.asp?lang=En&n=137E1147-0.]
Bonsal, B. R., A. Shabbarr, and K. Higuchi (2001), Impacts of low frequency variability modes on Canadian winter temperature, *Int. J. Climatol.*, *21*, 95–108, doi:10.1002/joc.590.
Bowen, G. J., and J. Revenaugh (2003), Interpolating the isotopic composition of modern meteoric precipitation, *Water Resour. Res.*, *39*(10), 1299, doi:10.1029/2003WR002086.
Bowen, G. J., and B. H. Wilkinson (2002), Spatial distribution of δ^{18}O in meteoric precipitation, *Geology*, *30*(4), 315–318, doi:10.1130/0091-7613(2002)030<0315:SDOOIM>2.0.CO;2.
Chun, K. P. (2010), Statistical downscaling of climate model outputs for hydrological extremes, PhD thesis, Dep. of Civ. and Environ. Eng., Imp. Coll. London, London, U. K.
Dansgaard, W. (1964), Stable isotopes in precipitation, *Tellus*, *16*(4), 436–468.
Davison, A., and D. Hinkley (1997), *Bootstrap Methods and Their Application*, Cambridge Univ. Press, Cambridge, U. K.
Delavau, C., T. A. Stadnyk, and S. J. Birks (2011), Model based distribution of oxygen-18 isotopes in precipitation across Canada, *Can. Water Resour. J.*, *36*(4), 313–330, doi:10.4296/cwrj3604875.
Durbin, J., and G. S. Watson (1951), Testing for serial correlation in least squares regression. 2., *Biometrika*, *38*, 159–178.
Dutton, A. L., B. H. Wilkinson, G. Bowen, J. M. Welker, and K. C. Lohmann (2005), Comparison of river water and precipitation δ^{18}O across the 48 contiguous United States, *Hydrol. Processes*, *19*, 3551–3572, doi:10.1002/hyp.5876.
Fisher, D. A., et al. (2004), Stable isotope records from Mount Logan and Eclipse ice cores and nearby Jellybean Lake; water cycle of the North Pacific over 2 000 years and over 5 vertical kilometres; sudden shifts and tropical connections, *Géogr. Phys. Quat.*, *58*, 337–52. doi:10.7202/013147ar.
Fischer M. J., and L. M. Baldini (2011), A climate-isotope regression model with seasonally-varying and time-integrated relationships, *Clim. Dyn.*, *37*(11-12), 2235–2251, doi:10.1007/s00382-011-1009-1.[10.1007/s00382-011-1009-1][Match].
Gat J. R., C. J. Bowser, and C. Kendall (1994), The contribution of evaporation from the Great Lakes to the continental atmosphere: Estimate based on stable isotope data, *Geophys. Res. Lett.*, *21*, 557–560, doi:10.1029/94GL00069.
Good, P. (2005), *Permutation, Parametric and Bootstrap Tests of Hydotheses*, 3rd ed., 315 pp., Springer, N. Y.
Harvey, F. E., and J. M. Welker (2000), Stable isotopic composition of precipitation in the semi-arid north-central portion of the US Great Plains, *J. Hydrol.*, *238*, 90–109, doi:1016/S0022-1694(00)00316-4.
International Atomic Energy Agency/World Meteorological Organization (2014), *Global Network of Isotopes in Precipitation, The GNIP Database*, Vienna, Austria. [Available at http://www.iaea.org/water.]
Kalkstein, L. S., M. C. Nichols, C. D. Barthel, and J. S. Greene (1996), A new spatial synoptic classification: Application to air-mass analysis, *Int. J. Climatol.*, *16*, 983–1004, doi:10.1002/(SICI)1097-0088(199609)16:9<983::AID-JOC61>3.0.CO;2-N.
Kottek, M., J. Grieser, C. Beck, B. Rudolf, and F. Rubel (2006), World Map of the Köppen-Geiger climate classification updated, *Meteorol. Z.*, *15*(3), 259–263, doi:10.1127/0941-2948/2006/0130.
Liebminger, A., G. Haberhauer, K. Varmuza, W. Papesch, and G. Heiss (2006), Modeling the oxygen 18 concentration in precipitation with ambient climatic and geographic parameters, *Geophys. Res. Lett.*, *33*, L05808, doi:10.1029/2005GL025049.
Lilliefors, H. W. (1967), On the Kolmogorov-Smirnov test for normality with mean and variance unknown, *J. Am. Stat. Assoc.*, *62*, 399–402, doi:10.2307/2283970.
Liu, Z., T. Lide, X. Chai, and T. Yao (2008), A model-based determination of spatial variation of precipitation δ18O over China, *Chem. Geol.*, *249*, 203–212, doi:10.1016/j.chemgeo.2007.12.011.
Liu, Z., G. Bowen, and J. M. Welker (2010), Atmospheric circulation is reflected in precipitation isotope gradients over the conterminous United States, *J. Geophys. Res.*, *115*, D22120, doi:10.1029/2010JD014175.
Liu, Z., G. Bowen, K. Yoshimura, K., and J. M. Welker (2013), Pacific North American teleconnection controls on precipitation isotopes (δ^{18}O) across the contiguous USA and adjacent regions, *J. Clim.*, *27*, 1046–1061, doi:10.1175/JCLI-D-13-00334.1.
Lykoudis, S. P., and A. A. Argiriou (2007), Gridded data set of the stable isotopic composition of precipitation over the eastern and central Mediterranean, *J. Geophys. Res.*, *112*, D18107, doi:10.1029/2007JD008472.
Lykoudis, S. P., A. A. Argiriou, and E. Dotsika (2010), Spatially interpolated time series of δ18O in Eastern Mediterranean precipitation, *Global Planet. Change*, *71*, 150–159 doi:10.1016/j.gloplacha.2009.09.004.
Mesinger, F., et al. (2006), North American regional reanalysis, *Bull. Am. Meteorol. Soc.*, *87*, 343–360, doi:10.1175/BAMS-87-3-343.
Peng, H., B. Mayer, S. Harris, and H. R. Krouse (2004), A 10-yr record of stable isotope ratios of hydrogen and oxygen in precipitation at Calgary, Alberta, Canada, *Tellus Ser. B*, *56B*, 147–159, doi:10.1111/j.1600-0889.2004.00094.x.
Peng, H., B. Mayer, S. Harris, and H. R. Krouse (2007), The influence of below-cloud secondary effects on the stable isotope composition of hydrogen and oxygen in precipitation at Calgary, Alberta, Canada. *Tellus Ser. B*, *59*, 698–704, doi:10.1111/j.1600-0889.2007.00291.x.
Peng, R. D., and F. Dominici (2008), *Statistical Methods for Environmental Epidemiology with R: A Case Study in Air Pollution and Health Series*, 144 pp., Springer, N. Y.
Rozanski, K., L. Araguás-Araguás, and R. Gonfiantini (1992), Relation between long-term trends of oxygen-18 isotope composition of precipitation and climate, *Science*, *258*, 981–985, doi:10.1126/science.258.5084.981.
Rozanski, K., L. Araguás-Araguás, and R. Gonfiantini (1993), Isotopic patterns in modem global precipitation, in *Climate Change in Continental Isotopic Records, Geophys. Monogr. Ser.*, vol. 78, edited by Swart, P. K. et al., pp. 1–36, AGU, Washington, D. C.
Sheridan, S. C. (2002), The redevelopment of a weather-type classification scheme for North America, *Int. J. Climatol.*, *22*, 51–68, doi:10.1002/joc.709.

Stadnyk, T. A., C. Delavau, N. Kouwen, and T. W. D. Edwards (2013), Towards hydrological model calibration and validation: Simulation of stable water isotopes using the isoWATFLOOD model, *Hydrol. Processes*, *27*, 3791–3810, doi:10.1002/hyp.9695.

Terzer, S., L. I. Wassenaar, L. J. Araguás-Araguás, and P. K. Aggarwal (2013), Global isoscapes for $\delta^{18}O$ and $\delta^{2}H$ in precipitation: Improved prediction using regionalized climatic regression models, *Hydrol. Earth Syst. Sci.*, *17*, 4713–4728, doi:10.5194/hess-17-4713-2013.

The MathWorks Inc. (2013), *MATLAB and Statistics Toolbox Release 2013a*, Natick, Mass.

Welker, J. M. (2000), Isotopic ($\delta^{18}O$) characteristics of weekly precipitation collected across the United States: An initial analysis with application to water source studies, *Hydrol. Processes*, *14*, 1449–1464, doi:10.1002/1099-1085(20000615)14:8<1449::AID-HYP993>3.0.CO;2-7.

Welker, J. M. (2012), ENSO effects on the isotopic (δ18O, δ2H and d-excess) of precipitation across the US using a long-term network (USNIP), *Rapid Comm. Mass Spec.*, *17*, 1655–1660, doi:10.1002/rcm.6298.

Wheeler, B. (2010), lmPerm: Permutation Tests for Linear Models. R Package Version 1.1–2. [Available at http://CRAN.R-project.org/package=lmPerm.] Accessed on August 10, 2014.

Vachon, R. W., J. W. C. White, E. Gutmann, and J. M. Welker (2007), Amount-weighted annual isotopic ($\delta^{18}O$) values are affected by the seasonality of precipitation: A sensitivity study, *Geophys. Res. Lett.*, *34*, L21707, doi:10.1029/2007GL030547.

Vachon, R. W., J. M. Welker, J. W. C. White, and B.H. Vaughn (2010a), Monthly precipitation isoscapes ($\delta^{18}O$) of the United States: Connections with surface temperatures, moisture source conditions, and air mass trajectories, *J. Geophys. Res.*, *115*, D21126, doi:10.1029/2010JD014105.

Vachon, R. W., J. M. Welker, J. W. C. White, and B.H. Vaughn (2010b), Moisture source temperatures and precipitation $\delta^{18}O$-temperature relationships across the US, *Water Resour. Res.*, *46*, W07523, doi:10.1029/2009WR008558.

Van der Veer, G., S. Voerkelius, G. Lorentz, G. Heiss, and J. A. Hoogewerff (2009), Spatial interpolation of the deuterium and oxygen-18 composition of global precipitation using temperature as ancillary variable, *J. Geochem. Explor.*, *101*, 175–184, doi:10.1016/j.gexplo.2008.06.008.

Yakir, D., and L. Sternberg (2000), The use of stable isotopes to study ecosystem gas exchange, *Oecologia*, *123*, 297–311, doi:10.1007/s004420051016.

Zhao, L., H. Xiao, M. Zhou, G. Cheng, L. Wang, L. Yin, and J. Ren (2011), Factors controlling spatial and seasonal distributions of precipitation $\delta^{18}O$ in China, *Hydrol. Processes*, *26*, 143–152, doi:10.1002/hyp.8118.